

# Rethinking Event-based Optical Flow: Iterative Deblurring as an Alternative to Correlation Volumes

Yilun Wu   Federico Paredes-Vallés   Guido C. H. E. de Croon

Micro Air Vehicle Laboratory, Technische Universiteit Delft

{Y.Wu-9, F.ParedesValles, G.C.H.E.deCroon}@tudelft.nl

## Abstract

Inspired by frame-based methods, state-of-the-art event-based optical flow networks rely on the explicit construction of correlation volumes, which are expensive to compute and store, at the same time prohibiting them from estimating high-resolution flow. We observe that the spatiotemporally continuous traces of events provide a natural search direction for seeking pixel correspondences, obviating the need to rely on gradients of explicit correlation volumes as such search directions. We introduce IDNet (Iterative Deblurring Network), a lightweight yet high-performing event-based optical flow network directly estimating flow from event traces without using correlation volumes. We further propose two iterative update schemes: “ID” which iterates over the same batch of events, and “TID” which iterates over time with streaming events in an online fashion. Benchmark results show the “ID” scheme outperforms previous state-of-the-art by 9% of EPE with 52% fewer parameters and 77% savings in memory footprint, while the “TID” scheme is even more efficient promising 80% of compute savings and 18 times less latency at the cost of only 6% of performance drop.

## 1. Introduction

Optical flow estimation, i.e. estimating the apparent motion vector of pixels through time on the image plane, is both a central and challenging task in computer vision. As it encodes a primitive form of motion information, optical flow serves as the backbone for many applications ranging from video compression [26, 43] and computational photography [22, 42] to robotic navigation [4, 33]. Traditionally, optical flow is estimated from frame-based cameras with methods ranging from hand-crafted optimization [16, 28] to modern learning-based methods [7, 38, 41]. Compared to frame-based cameras, event cameras capture asynchronous brightness changes in continuous time, of-

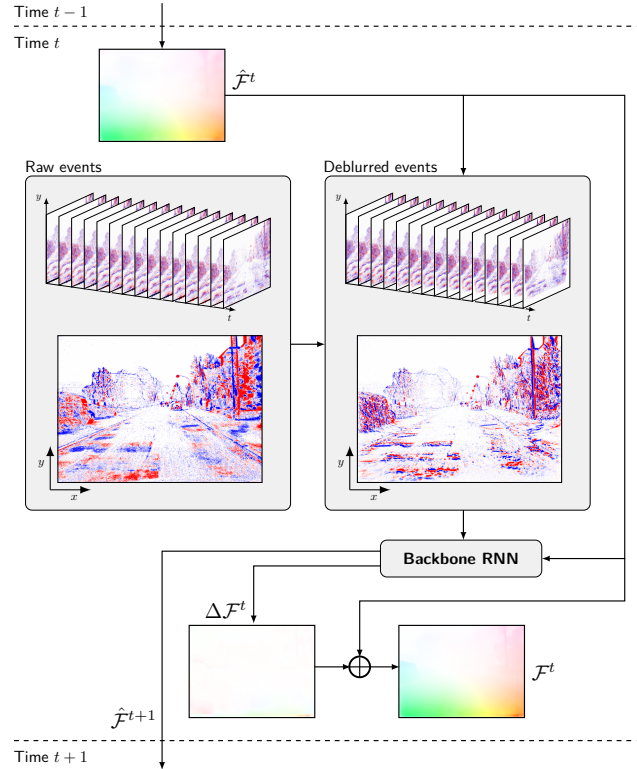


Figure 1. Illustration of the IDNet pipeline for temporal iterative deblurring (i.e. TID scheme). Raw events are first deblurred according to the initial coarse optical flow estimate  $\hat{\mathcal{F}}^t$  before being processed by the backbone RNN. The RNN extracts the residual motion from the deblurred events and outputs the residual flow  $\Delta \mathcal{F}^t$  which is added to the initial estimate  $\hat{\mathcal{F}}^t$  to arrive at the final flow estimation  $\mathcal{F}^t$ . The RNN additionally proposes a coarse estimate  $\hat{\mathcal{F}}^{t+1}$  for the next timestep under continuous operation.

fering high dynamic range measurements free from motion blur even at high speeds and low lighting conditions [9]. In addition, such a data format is superior for estimating optical flow, as the trajectory of motion is captured continuously in the data stream instead of being captured in discrete pixel locations across two frames.

Under review. Code and models will be released upon acceptance.

The advances in the recent performance of learning-based methods for optical flow estimation can be seen as the process of incorporating ever more fitting inductive biases to the underlying problem. PWC-Net [38] introduces pyramid processing, warping, and cost volume, three common ingredients used in classical model-based methods, and achieved superior performance with a much smaller network compared to its predecessor [7]. RAFT [41] further improves the performance by replacing the optimization process in finding maximum correlation with an RNN iteratively operating over the all-pair cost volume.

Recently, an event-based version of RAFT, termed E-RAFT [13], has been developed. The method applied the RAFT architecture to event data by treating two event representations consecutive in time as two images in the context of estimating flow from frames. E-RAFT achieves state-of-the-art performance on the challenging event-based optical flow benchmark DSEC [12], demonstrating the strong effectiveness of appropriate inductive biases (i.e. correlation and iterative optimization) for this problem.

However, we note that there are three major drawbacks of the method when applied to event data. First, the multi-bin event representation cannot be processed one bin at a time, prohibiting parallel computation as events arrive. This prevents the algorithm from real-time operations under tight latency constraints. Second, computing and storing the all-pair correlation volume is expensive, making it difficult to deploy on memory/compute-limited systems for inference. Finally, as noted in [23, 44], the correlation volume scales poorly to higher input resolutions, limiting the algorithm’s ability to deliver fine details in optical flow estimates.

We observe that, compared to estimating flow from two images, event-based optical flow benefits from the continuous recording of motion over time and space. This additional information enables us to estimate flow by simply tracing the continuous trajectory, whereas frame-based methods have to search for such “trajectory” by estimating gradients in the all-pair correlation volume. In other words, while correlation volumes are necessary for methods operating over frames to propose an update direction, such direction is readily available in the form of blur (i.e. the continuous spatiotemporal trajectory) in the raw events.

Based on this observation, we propose *IDNet* (Iterative Deblurring Network), an event-based algorithm for iterative optical flow estimation without correlation volumes. At its core, *IDNet* processes event bins sequentially via a backbone RNN where optical flow is estimated from the traces (i.e. blur) of input events. In addition, we adopt an iterative update scheme that can both handle fast motion and preserve fine details. To achieve this, we utilize the principle of motion compensation (a.k.a. deblurring), as introduced in [10]. At each iteration, we deblur the raw events based on the previous flow estimate and process them with the

same backbone network to extract the residual optical flow for updating the flow estimate. This is similar to warping operations in frame-based optical flow, where a coarse flow is used to warp the target image before refinement.

We propose two iterative update schemes: *ID* (iterative deblurring), illustrated in Fig. 2, which iterates over the same batch of events to achieve the best performance, and *TID* (temporal iterative deblurring), shown in Fig. 1, which iterates over events in time for drastically faster processing.

On public benchmarks, our methods achieve comparable results with state-of-the-art methods that use correlation volumes, while using much fewer parameters and memory. Without correlation volumes, our method can estimate optical flow from higher-resolution feature maps, resulting in significant improvements over prior art. Additionally, our *TID* scheme is highly efficient, reaching close-to-state-of-the-art performance while incurring minimal latency.

## 2. Related Works

### 2.1. Event-based Optical Flow

Traditionally, optical flow estimation is performed from image frames with algorithms ranging from classical optimization techniques such as [16, 28] to modern learning-based methods [7, 19, 34, 38, 41] which combine the powerful expressivity of deep neural networks with inductive biases such as correlation matching and coarse-to-fine estimation. While frame-based optical flow estimation has reached a mature stage after decades of research, there are scenarios where images would suffer from quality degradation, such as motion blur and insufficient exposure.

Event cameras, on the other hand, are not plagued by such issues and hence are more suited for use in these challenging conditions. This has led to increased adoption of such sensors in the industry and a growing interest in event-based optical flow among the research community.

The early event-based optical flow algorithm [3] adapts frame-based methods such as KLT [28] to the event-based domain or utilizes hand-crafted heuristics to fit event data [2, 29]. [1] jointly optimizes image brightness and optical flow by exploiting brightness constancy, flow smoothness and the event generation model together. [10, 36] introduces a framework to recover optical flow from events by maximizing the contrast of motion-compensated events. Other than directly optimizing the objective, this principle is also applied as a learning signal in self-supervised learning methods such as [14, 31, 45, 46].

The availability of event simulators [11, 18] and large-scale datasets [12, 47] enable learning-based methods to achieve superior performance over model-based ones. [46] introduces an event representation which split events proportionally to the nearby temporal bins and a U-Net architecture for processing the event representation. [45] jointly



estimates optical flow, depth and egomotion. Both methods construct multi-level feature pyramids and [45] warps the event representation slices to evaluate the quality of flow through the contrast maximization framework. E-RAFT [13], an event-based version of RAFT [41] is the first learning-based method to introduce correlation volumes into the event domain. The method computes the 4D all-pair correlation volume between two neighboring event representations in time, which is then iteratively processed through an RNN to arrive at the final optical flow estimate.

Although E-RAFT achieves state-of-the-art performance while being relatively lightweight compared to previous learning-based methods, the explicit computation and storage of all-pair correlation volume, as mentioned in [23, 44], has poor time and storage complexity which scales badly with input resolution. For two event representations of size  $C \times H \times W$ , the compute and storage complexity of such correlation volume is  $\mathcal{O}((H \times W)^2 \times C)$  and  $\mathcal{O}((H \times W)^2)$  respectively. This storage requirement eliminates the possibility of its deployment on memory-limited compute platforms and prohibits the algorithm from scaling up to larger input resolutions.

## 2.2. Iterative Refinement for Optical Flow

The idea of iterative refinement for optical flow can be traced back to the early works of iterative KLT tracking [28] where a Taylor series expansion is applied to linearize the problem and iteratively solve for the residual error. Learning-based methods incorporate this principle as well. Most works [34, 38, 19] choose to perform coarse-to-fine refinement along the feature pyramid. In addition to spatial refinement, other works such as [20, 21, 27, 41] stack multiple modules in series to iteratively estimate the residual flow from representations warped by the current flow estimate. While [21] warps images, [20] and [41] sample correlation volumes and [27] recomputes correlation volumes. [20, 27, 41] share weights of the refinement modules, making their architecture recurrent rather than feed-forward.

Recently, iterative refinement for optical flow has also been applied to event-based data. [17] and [25] use pyramid scale to perform coarse-to-fine estimation similar to PWC-Net [38] but do not perform flow refinement through iterations. [6] adopts the update scheme in [20] and processes the correlation volume between warped event slices through time to arrive at a residual flow estimate. [13] instead directly processes the all-pair correlation volume through an RNN and extracts the final flow estimate from the state of the RNN at the end of its iterations. All aforementioned methods rely on the explicit construction of correlation volumes as a basis for their refinement schemes.

## 2.3. Continuous Operation

Since optical flow is temporally highly correlated as the motion in a real-world environment is mostly smooth and continuous, it makes sense to leverage the prior estimate from the past to better predict the present optical flow. This temporal recurrency is introduced in [30] and used in RAFT [41] as a “warm-starting” strategy when applied to video data. RAFT [41], as well as E-RAFT [13], directly transports the previous flow field to the current timestep by the flow itself under the assumption of constant linear motion.

## 3. Methodology

### 3.1. Problem Formulation

We define the problem of optical flow estimation as the mapping from a sequence of event streams containing triggering timestamp  $t$ , pixel location  $x, y$  and binary polarity  $p$  in a time window:  $\{e_i = (t_i, x_i, y_i, p_i)\}$ , where  $t_i \in [t_{\text{begin}}, t_{\text{end}}]$  to a dense optical flow vector for every pixel:  $(u, v)$ , which is the two-dimensional flow defined at time  $t = t_{\text{begin}}$ . As in [13, 48], we utilize the discretized event volume as the event representation, which interpolates each event into its two adjacent bins weighted by its timestamp and polarity.

Specifically, we create a representation  $\mathcal{E} \in \mathbb{R}^{B \times H \times W}$  with  $B$  bins out of the event stream  $\{e_i = (t_i, x_i, y_i, p_i)\}$  of interest as follows:

$$t_i^* = (B - 1)(t_i - t_{\text{begin}})/(t_{\text{end}} - t_{\text{begin}}) \quad (1)$$

$$\mathcal{E}(B, x, y) = \sum_{i|x_i=x, y_i=y} p_i \max(0, 1 - |B - t_i^*|) \quad (2)$$

where  $H, W$  correspond to the height and width resolution of the event stream respectively.

### 3.2. Motion Compensation

As introduced in [10], we utilize the principle of motion compensation as a core step in our processing. Specifically, we use the flow estimate  $\mathcal{F}$  to deblur the events to a reference time  $t_{\text{ref}}$  by changing its pixel coordinate  $\mathbf{x}_i = (x_i, y_i)$  in the following way:

$$\mathbf{x}'_i = \mathbf{x}_i + (t_{\text{ref}} - t_i)\mathcal{F}(x_i) \quad (3)$$

Ideally, under the assumption of brightness constancy and linear motion, the ideal flow would cancel out all the motion in the events, leading to a static event representation without any motion. An illustration of the comparison before and after such motion compensation can be seen in Fig. 1. The collapsed view where all bins of the event representation  $\mathcal{E}$  are projected onto the same 2D plane reveals that the deblurred events exhibit less motion and moving objects appear static and preserve sharp edges.

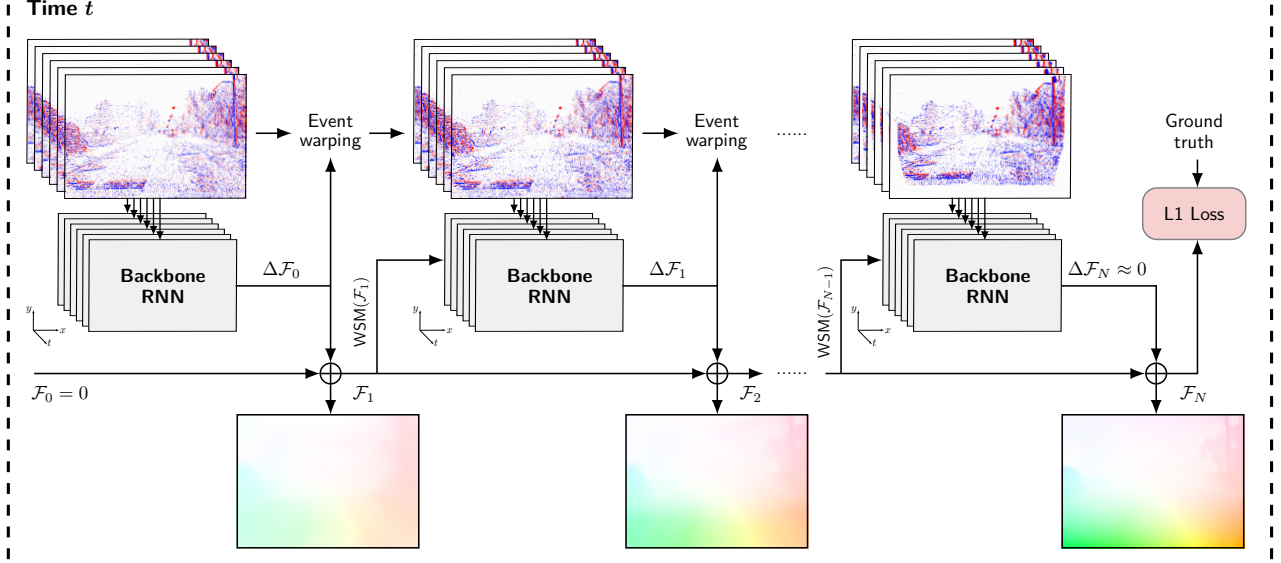


Figure 2. Overall pipeline of *IDNet* with iterative deblurring scheme (i.e. *ID* scheme). At the beginning of iterations, a zero flow estimate is initiated. At each iteration, the previous flow estimate is used to deblur events. The deblurred event bins are fed into the RNN sequentially one bin at a time. A residual flow is estimated and used for deblurring in the next iteration. The final flow is the sum of all predicted residual flows throughout iterations. Finally, an L1 loss is enforced between the final flow estimate and ground truth.

### 3.3. Iterative Deblurring

The main architecture of *IDNet* under iterative deblurring (*ID* scheme) is shown in Fig. 2. The backbone of our proposed *IDNet* is a recurrent neural network which processes the input event bins sequentially one bin at a time. An optical flow field is read out from the state of the RNN once all bins have been passed through it. In this case, we select a ConvGRU as the choice for the recurrent unit.

Next, we introduce iterative deblurring on top of the sequential processing described above. The design here is inspired by the predictive coding scheme in the visual cortex [35], where the belief of the world is iteratively updated and only the error signal, i.e. the difference between the visual input signal and the predicted signal according to the current belief, is sent to the visual cortex for refining belief until equilibrium. We take a similar approach by using motion compensation as the prediction model to iteratively refine the flow from the residual signal.

An overview of the algorithm is presented in Algorithm 1. Specifically, as shown in Fig. 2, we initialize our flow estimate as well as the memory of the backbone RNN to be zero at the beginning ( $\mathcal{F}_0 = \mathbf{0}$ ,  $\mathcal{M}_{\text{RNN},0} = \mathbf{0}$ ). Once the backbone RNN makes a prediction  $\mathcal{F}_1$  of the flow from the raw event bins  $\mathcal{E}_0$ , the event bins are motion-compensated with the optical flow vector  $\mathcal{F}_1(x_i)$ , resulting in partially deblurred event bins  $\mathcal{E}_1$ . We then start the next iteration of refinement by passing  $\mathcal{E}_1$  into the backbone network for another round of flow prediction. As the number of iterations increases, the flow refinement approaches zero.

---

#### Algorithm 1: Iterative deblurring (*ID*).

---

**input** : Event bins  $\mathcal{E}$  containing events in a time window of duration  $T$   
Number of deblurring iterations  $N$   
**output**: Optical Flow Prediction  $\mathcal{F}$  for the motion during the time window of events

$\mathcal{F}_0 \leftarrow \mathbf{0}$ ,  $\mathcal{M}_{\text{RNN},0} \leftarrow \mathbf{0}$ ,  $\mathcal{E}_{\text{deblur},0} \leftarrow \mathcal{E}$   
**for**  $i \leftarrow 0; i < N; i++$  **do**  
     $\Delta\mathcal{F}_i \leftarrow \text{RNN}(\text{Encoder}(\mathcal{E}_{\text{deblur},i}); \mathcal{M}_{\text{RNN},i})$   
     $\mathcal{F}_{i+1} \leftarrow \mathcal{F}_i + \Delta\mathcal{F}_i$   
     $\mathcal{M}_{\text{RNN},i+1} \leftarrow \text{WarmStartModule}(\mathcal{F}_{i+1})$   
     $\mathcal{E}_{\text{deblur},i+1} \leftarrow \text{Deblur}(\mathcal{E}_{\text{deblur},i}; \Delta\mathcal{F}_i)$   
 $\mathcal{F} \leftarrow \mathcal{F}_N$   
**return**  $\mathcal{F}$

---

To leverage the RNN’s recurrency, we use a warm-starting module (WSM) comprising feed-forward convolutional layers to initialize the memory of our backbone RNN:  $\mathcal{M}_{\text{RNN},1} = \text{WSM}(\mathcal{F}_1)$ . This time, we update the previous belief by adding the residual flow  $\Delta\mathcal{F}_2$  estimated from  $\mathcal{E}_1$  to the previous belief  $\mathcal{F}_1$  to arrive at the flow estimate at iteration 2:  $\mathcal{F}_2 = \mathcal{F}_1 + \Delta\mathcal{F}_2$ , from which a new iteration could be started again.

Weight sharing the RNN for all iterations is motivated by the expectation that the backbone network can extract any residual motion in the event representation, raw or deblurred, rendering the task unchanged across iterations.

### 3.4. Iterative Deblurring through Time

We also explore another mode of iterative refinement through the temporal scale, as shown in Fig. 1. Instead of deblurring the same events multiple iterations, we give the network access to a continuous stream of events where at each timestep we deblur the event bins  $\mathcal{E}^t$  and pass the deblurred bins  $\mathcal{E}_{\text{deblur}}^t$  through the backbone RNN only once. In addition to estimating the optical flow  $\mathcal{F}^t$  for the current timestep, we predict an initial flow  $\hat{\mathcal{F}}^{t+1}$  for deblurring the event bins  $\mathcal{E}^{t+1}$  from the next timestep. This recurrent connection allows the network to refine the flow and compose a finer prior over time, as demonstrated in Fig. 3. The key difference between running this pipeline vs simply passing the raw unblurred event bins through the backbone network once, is that our pipeline initializes an informative memory from previous estimates and only processes deblurred event bins with smaller motion range. This enables the backbone RNN to improve flow accuracy at a finer scale with limited parameters.

Operational-wise, we utilize the same principle of motion compensating events and warm starting the memory of RNN as before, but introduce an additional module to estimate the initial flow for the following timestep  $\hat{\mathcal{F}}^{t+1}$  through the state of the backbone RNN. A pseudo code of the algorithm is laid out in Algorithm 2.

---

#### Algorithm 2: Temporal iterative deblurring (TID).

---

**input :** Event bins  $\mathcal{E}^t$  containing events with  $\tau \in [t, t + T]$   
Initial flow estimate at  $\hat{\mathcal{F}}^t$  at time  $t$   
**output:** Optical Flow Prediction  $\mathcal{F}^t$  at time  $t$  for the motion from  $\tau \in [t, t + T]$

$\mathcal{M}_{\text{RNN}}^t \leftarrow \text{WarmStartModule}(\hat{\mathcal{F}}^t)$   
 $\mathcal{E}_{\text{deblur}}^t \leftarrow \text{Deblur}(\mathcal{E}^t; \hat{\mathcal{F}}^t)$   
 $\Delta\mathcal{F}^t, \hat{\mathcal{F}}^{t+1} \leftarrow \text{RNN}(\text{Encoder}(\mathcal{E}_{\text{deblur}}^t); \mathcal{M}_{\text{RNN}}^t)$   
 $\mathcal{F}^t \leftarrow \hat{\mathcal{F}}^t + \Delta\mathcal{F}^t$   
**return**  $\mathcal{F}^t, \hat{\mathcal{F}}^{t+1}$

---

### 3.5. Network Architecture

We select a single layer of ConvGRU with 96 feature channels as our backbone network. The `Encoder` network, which consists of 9 convolutional layers with 4 layers adding a residual connection, produces 64-dim lower-resolution feature maps from each full-resolution event bin before being processed by the backbone RNN. The RNN outputs a lower-resolution flow field which is upsampled back to the original input size via convex upsampling, similar to [13, 41]. The `WSM` module takes the same architecture as the `Encoder` network. See the Appendix D for module architecture details.



Figure 3. Initial flow  $\hat{\mathcal{F}}^t$ , residual flow  $\Delta\mathcal{F}^t$  and final flow  $\mathcal{F}^t$  as time progresses and new event bins keeps coming. A trend of increasing quality in  $\mathcal{F}^t$  and lowering magnitude in  $\Delta\mathcal{F}^t$  can be observed, implying that the flow is iteratively refined through time.

### 3.6. Loss

For the update scheme of iterative deblurring (*ID*), we apply L1 loss between the final flow and ground truth:

$$\mathcal{L}_{\text{ID}} = \|\mathcal{F}_{\text{gt}} - \mathcal{F}_N\|_1 \quad (4)$$

For training temporal iterative deblurring (*TID*), we take a prediction sequence of length  $T$  and enforce an L1 loss on both the intermediate current flows and future flows and weigh them using a geometric series to penalize error more on later iterations, where  $\gamma \in (0, 1)$ :

$$\mathcal{L}_{\text{TID}} = \sum_{t=0}^T \gamma^{T-t} (\|\mathcal{F}_{\text{gt}}^t - \mathcal{F}^t\|_1 + \|\mathcal{F}_{\text{gt}}^{t+1} - \hat{\mathcal{F}}^{t+1}\|_1) \quad (5)$$

## 4. Experiments

### 4.1. Training Details

We train and evaluate our models on the DSEC Optical Flow dataset [12] [13]. We set the number of deblurring iterations  $N$  to be 4 for Algorithm 1 and the sequence length  $T = 4$  and  $\gamma = 0.8$  in Eq. (5). We use an event representation with  $B = 15$  bins for every 100 ms of events, aligned with the available optical flow ground truth. We train our models implemented with PyTorch [32] on NVIDIA RTX 3090 and A100 GPUs. We use the Adam [24] optimizer with the onecycle learning rate scheduler [37] under a maximum learning rate of  $1 \times 10^{-4}$  and a batch size of 3 for 250K steps. To account for the longer-duration event trajectories which span greater distances on the image plane, we apply random cropping to a larger size of 384 by 512 for training *TID* models, compared to the 288 by 384 size used for *ID* models. We also apply horizontal flipping and a 10% probability of vertical flipping as data augmentation during training. On MVSEC, we finetune our models on the `outdoor_day_2` sequence with horizontal flipping for 500 steps before evaluation on the `outdoor_day_1` sequence.

	Performance					Model Statistics		
	EPE	AE	1PE	2PE	3PE	Model Size	GMAC	Memory Footprint
MultiCM [36]	3.47	13.98	76.6	48.4	30.9	-	-	-
EV-FlowNet [46]	2.32	7.90	55.4	29.8	18.6	14M	358	120MB
OF_EV_SNN [5]	1.71	6.34	53.7	20.2	10.3	<b>1.2M</b>	-	56MB
E-RAFT [13] (1/8 Resolution)	<u>0.79</u>	<u>2.85</u>	12.7	4.7	2.7	5.3M	256	132MB
└ E-RAFT (1/4 Resolution)	GPU Out of Memory (>40GB)					5.3M	750	1.9GB
└ E-RAFT w/o Correlation Volume	1.20	3.75	27.5	11.5	6.3	4.5M	208	40MB
<b>Ours (ID, 4 iterations, 1/4 Resolution)</b>	<b>0.72</b>	<b>2.72</b>	<b>10.1</b>	<b>3.5</b>	<b>2.0</b>	2.5M	550	<u>30MB</u>
<b>Ours (ID, 4 iterations, 1/8 Resolution)</b>	<u>0.79</u>	2.91	<u>12.1</u>	<u>4.3</u>	<u>2.4</u>	<u>1.4M</u>	<u>222</u>	<b>20MB</b>
<b>Ours (TID, 1 iteration, 1/8 Resolution)</b>	0.84	3.41	14.7	5.0	2.8	1.9M	<b>55</b>	<b>20MB</b>

Table 1. Evaluation on DSEC-Flow dataset with model statistics. The best metric is in bold, while the second best is underlined. Upscaled E-RAFT does not fit in our A100 GPU with 40GB of VRAM for training.

## 4.2. Benchmark Results

Our quantitative evaluations on DSEC and MVSEC are presented in Table 1 and Table 3. We report the following metrics as well as model statistics: EPE (Endpoint error), which is the average of the L2-Norm of the optical flow error vector in pixels; AE (Angular error), which is the average of the angular error of the optical flow vector in degrees; nPE (n-pixel outlier percentage), which is the percentage of pixels with optical flow magnitude error greater than n pixels. Additionally, we report the model size in millions of parameters; GMAC, the number of Giga multiply-and-accumulation operations required for estimating one optical flow during inference measured in billions of operations, and finally its memory footprint, the minimum amount of working memory required during inference while executing the computation graph of the model for one sample.

On the DSEC-Flow benchmark, as shown in Table 1, E-RAFT [13] is the only method that achieves comparable performance to our models. When processing feature maps of 1/8th the input resolution, *ID* performs on-par with E-RAFT while using a quarter of the parameters and 15% of the memory during execution. These memory savings are due to a smaller network but mainly due to the elimination of the need to store the all-pair correlation volume used by E-RAFT, which is essential to its performance. Removing the correlation volume from E-RAFT results in a smaller memory footprint but significantly deteriorated performance, illustrating its importance.

As pointed out in [23, 44], all-pair correlation volumes have poor time and space complexity, necessitating construction from feature maps with 1/8 the resolution of the input size to ensure reasonable memory usage. This limitation impacts performance, as fine details cannot be preserved in low-resolution features. As a concrete example, E-RAFT processing 1/4 resolution would consume 2GB of memory

	EPE	Latency	Processing Mode
E-RAFT [13]	0.79	55ms	Batch
<b>Ours (TID)</b>	0.84	3ms	On-the-fly

Table 2. EPE, latency and processing mode of E-RAFT and *TID* methods, measured on RTX 3090 GPU.

per example, making it not only impractical to deploy on most hardware but also impossible to train on a single GPU due to the even larger memory requirement for training. In contrast, *IDNet* can scale easily to higher-resolution feature maps. After adjusting the stride of convolution layers in the *Encoder* module to generate 1/4 resolution feature maps, performance immediately improves by 9% on EPE, surpassing the previous state-of-the-art result on this benchmark.

The benefits of upscaled feature maps would also generalize to correlation-volume-based methods. We train a non-recurrent E-RAFT with upscaled features that fits on our GPU with less memory consumption during training. Although a performance boost is similarly observed, it still underperforms our method while consuming 60x more memory usage. Refer to Appendix C for the detailed metrics.

While *ID* performs better, *TID* is drastically faster by only iterating once. By leveraging the temporal prior, we have managed to retain almost the full quality of prediction while incurring a performance drop of only 6% compared to 4 iterations of *ID* and prior art method E-RAFT, which consumes nearly 5 times more compute. Moreover, E-RAFT requires accumulating all events in a time window before processing, resulting in high latency, while *TID* processes event bins sequentially and can thus parallelize the processing of bins as events arrive in real-time, significantly reducing inference latency, as reported in Table 2.

On the MVSEC dataset, as shown in Table 3, our meth-





Figure 4. Qualitative results of optical flow predictions on DSEC-Flow with highlighted regions of interest. Images are for visualization only, as optical flow is event-based. Samples taken from the test sequences show that our *ID* method at 1/4 resolution produces superior results on fine details and small objects, while the *TID* method yields results that are comparable to those of E-RAFT.

	EPE	1PE	3PE
EV-FlowNet [46]	0.61	15.6	0.45
E-RAFT [13]	<u>0.47</u>	9.2	<u>0.24</u>
<b>Ours (ID, 1/4 Resolution)</b>	0.49	9.9	<u>0.24</u>
<b>Ours (ID, 1/8 Resolution)</b>	<b>0.46</b>	<b>7.9</b>	0.25
<b>Ours (TID, 1/8 Resolution)</b>	<u>0.47</u>	<u>9.1</u>	<b>0.20</b>

Table 3. Evaluation on MVSEC dataset *outdoor\_day\_1* sequence with 20Hz update rate. The best metric is in bold, while the second best is underlined.

ods perform on-par with E-RAFT [13]. Interestingly, scaling up the resolution did not yield a boost but rather a slight drop in performance, unlike the case in the DSEC benchmark. We speculate this is due to the small amount of training data available which renders the larger model more difficult to generalize.

### 4.3. Qualitative Results

Fig. 4 presents examples of optical flow predictions taken from different test sequences of DSEC-Flow. We observe that our *ID* method with increased resolution enhances the recovery of fine details in regions with intricate structures, such as the guardrail in the *interlaken\_01\_a* sequence and the forearm of the walking pedestrian in *zurich\_city\_15\_a*. Furthermore, our method preserves sharper motion boundaries, which is evident in the traffic sign of *zurich\_city\_12\_a* as well as the excavator arm in *interlaken\_00\_b*, where only our *ID* methods predicted its contour accurately.

On the other hand, our *TID* method delivers optical flow estimates of comparable quality to those of E-RAFT. In less challenging conditions, the *TID* method’s performance is difficult to distinguish from our *ID* methods. Additional visualizations can be found in Appendix G.

	EPE	AE	1PE	3PE
ID 4 iters	<b>0.88</b>	<b>3.21</b>	<b>15.6</b>	<b>3.2</b>
ID 2 iters	0.94	3.43	18.1	3.7
ID 1 iter	1.30	4.82	33.7	6.7
ID 4 iters w/o deblurring	1.24	4.49	31.1	6.6
ID 4 iters w/o WSM	1.02	4.07	20.8	4.0

Table 4. Ablation study on DSEC-Flow w.r.t the effectiveness of iterative deblurring. The study uses a slightly scaled-down model than the ones presented in Table 1.

	EPE	AE
<i>TID</i> w/ Direct Transport	1.25	4.60
<i>TID</i> w/ Learning	0.93	3.98
E-RAFT w/ Direct Transport	0.79	2.85
E-RAFT w/ Learning	-	-

Table 5. Impact of direct vs learned forward propagation schemes on *TID* and E-RAFT.

#### 4.4. Ablation Studies

**Iterative refinement and Deblurring** We study the impact of introducing iterative deblurring on a slightly scaled-down model to save time and resources. The results are reported in Table 4. For this experiment, we first set the number of deblurring iterations down to 1. Without either iterative processing or deblurring, the performance dropped by 47% on EPE. Introducing recurrency with 4 iterations but no deblurring, where the network would take raw event bins instead of the deblurred ones as outlined in Algorithm 1, results in a 41% decrease in EPE, demonstrating the effectiveness of deblurring as an inductive bias. Lastly, we remove the warm starting module so that the memory of the backbone RNN would be initialized to zero for all iterations. This time, EPE and AE went up by roughly 16%, revealing the recurrency is better complemented with an informative prior provided to the backbone RNN.

We also study the impact of the number of deblurring iterations on the performance by comparing *ID* models with  $N = 1, 2, 4$  iterations. We observe that iterating twice already lowers EPE by 27%, while two extra deblurring iterations bring a diminishing further improvement of 5%.

**Forward Propagation Methods** Previous methods such as E-RAFT[13] use warping to warm start the prediction for the next timestep, which simply transports the optical flow vector estimated from the current timestep by itself to arrive at a coarse estimate for the next timestep. However, even with the high quality flow predictions made by E-RAFT, directly transporting those will lead to artifacts shown in Fig. 5, such as the white regions with zero flow caused by

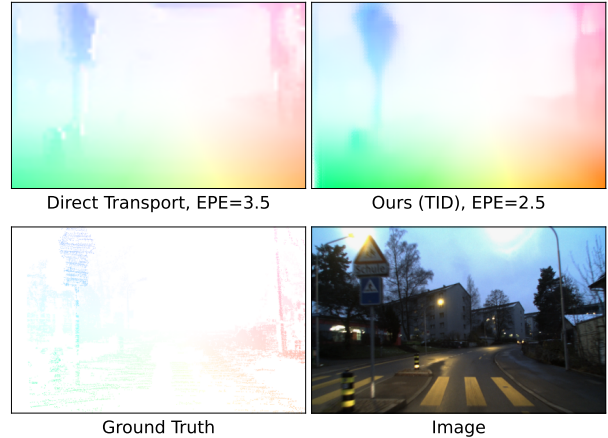


Figure 5. Comparison of optical flow propagation schemes. The flow prediction made by direct transport from E-RAFT [13] suffers from artifacts due to occlusion while our learning-based approach yields a smooth optical flow field with lower EPE error.

occlusion. Instead, we propose to learn future flow directly as described in Algorithm 2. This approach improves the accuracy of future flow prediction and when combined with *TID*, gives a significant 25% boost in the performance on DSEC-Flow, as shown in Table 5. Interestingly, replacing the direct transport scheme with a learning-based prediction on E-RAFT does not lead to effective training, possibly due to its update module’s specialization in predicting only the current optical flow.

## 5. Conclusion

The huge success of correlation volumes in frame-based optical flow has led the majority of recent event-based optical flow methods to adopt it. We contend that such methods suffer from significant memory consumption drawbacks, impeding their deployment and restricting their performance based on the resolution of feature maps they can process. We further observe that the spatiotemporal event traces can serve as a viable search direction during iterative refinement, rendering the correlation volume obsolete for proposing search directions via its gradient. We demonstrate the aforementioned approach through *IDNet*, a lightweight yet high-performing event-based optical flow method without using correlation volumes.

We demonstrate through experiments that iterative deblurring can serve as a superior alternative to correlation-volume-based approaches due to its lightweight design, low memory usage, scalability to high resolution, compatibility with on-the-fly processing, and ability to maintain high performance. We believe our work provides valuable insights into efficiently solving event-based optical flow problems and hope to encourage the community to explore such a combination for other architectures and vision tasks.

## Acknowledgements

This work was sponsored by the Office of Naval Research (ONR) Global under grant number N629092112014. The views and conclusions contained herein are those of the authors only and should not be interpreted as representing those of the U.S. Government.

## References

- [1] Patrick Bardow, Andrew J. Davison, and Stefan Leutenegger. Simultaneous optical flow and intensity estimation from an event camera. In *2016 IEEE Conference on Computer Vision and Pattern Recognition (CVPR)*, pages 884–892, 2016. 2
- [2] Ryad Benosman, Charles Clercq, Xavier Lagorce, Sio-Hoi Ieng, and Chiara Bartolozzi. Event-based visual flow. *IEEE Transactions on Neural Networks and Learning Systems*, 25(2):407–417, 2014. 2
- [3] Ryad Benosman, Sio-Hoi Ieng, Charles Clercq, Chiara Bartolozzi, and Mandyam Srinivasan. Asynchronous frameless event-based optical flow. *Neural Networks*, 27:32–37, 2012. 2
- [4] Haiyang Chao, Yu Gu, and Marcello Napolitano. A survey of optical flow techniques for robotics navigation applications. *Journal of Intelligent & Robotic Systems*, 73(1):361–372, 2014. 1
- [5] Javier Cuadrado, Ulysse Rançon, Benoît Cottureau, Francisco Barranco, and Timothée Masquelier. Optical flow estimation with event-based cameras and spiking neural networks, 2023. 6
- [6] Ziluo Ding, Rui Zhao, Jiyuan Zhang, Tianxiao Gao, Ruiqin Xiong, Zhaofei Yu, and Tiejun Huang. Spatio-temporal recurrent networks for event-based optical flow estimation. In *Proceedings of the AAAI Conference on Artificial Intelligence (AAAI)*, volume 36, pages 525–533, 2022. 3
- [7] Alexey Dosovitskiy, Philipp Fischer, Eddy Ilg, Philip Häusser, Caner Hazirbas, Vladimir Golkov, Patrick van der Smagt, Daniel Cremers, and Thomas Brox. FlowNet: Learning optical flow with convolutional networks. In *2015 IEEE International Conference on Computer Vision (ICCV)*, pages 2758–2766, 2015. 1, 2
- [8] Semiconductor Engineering. Memory issues for ai edge chips. <https://tinyurl.com/memedge>, March 2020. 13
- [9] G. Gallego, T. Delbruck, G. Orchard, C. Bartolozzi, B. Taba, A. Censi, S. Leutenegger, A. J. Davison, J. Conrads, K. Daniilidis, and D. Scaramuzza. Event-based vision: A survey. *IEEE Transactions on Pattern Analysis and Machine Intelligence*, 44(01):154–180, 1 2022. 1
- [10] Guillermo Gallego, Henri Rebecq, and Davide Scaramuzza. A unifying contrast maximization framework for event cameras, with applications to motion, depth, and optical flow estimation. In *2018 IEEE/CVF Conference on Computer Vision and Pattern Recognition*, pages 3867–3876, 2018. 2, 3
- [11] Daniel Gehrig, Mathias Gehrig, Javier Hidalgo-Carrio, and Davide Scaramuzza. Video to events: Recycling video datasets for event cameras. *2020 IEEE/CVF Conference on Computer Vision and Pattern Recognition (CVPR)*, 6 2020. 2
- [12] Mathias Gehrig, Willem Aarents, Daniel Gehrig, and Davide Scaramuzza. Dsec: A stereo event camera dataset for driving scenarios. *IEEE Robotics and Automation Letters*, 6(3):4947–4954, 2021. 2, 5, 13
- [13] Mathias Gehrig, Mario Millhäusler, Daniel Gehrig, and Davide Scaramuzza. E-raft: Dense optical flow from event cameras. In *International Conference on 3D Vision (3DV)*, 2021. 2, 3, 5, 6, 7, 8, 11, 14
- [14] Jesse Hagenaars, Federico Paredes-Valles, and Guido de Croon. Self-supervised learning of event-based optical flow with spiking neural networks. In M. Ranzato, A. Beygelzimer, Y. Dauphin, P.S. Liang, and J. Wortman Vaughan, editors, *Advances in Neural Information Processing Systems*, volume 34, pages 7167–7179. Curran Associates, Inc., 2021. 2
- [15] Bas J. Hordijk, Kirk Y. Scheper, and Guido C. H. E. de Croon. Vertical landing for micro air vehicles using event-based optical flow. *Journal of Field Robotics*, 35(1):69–90, 2018. 13
- [16] Berthold K.P. Horn and Brian G. Schunck. Determining optical flow. *Artificial Intelligence*, 17(1):185–203, 1981. 1, 2
- [17] Liwen Hu, Rui Zhao, Ziluo Ding, Lei Ma, Boxin Shi, Ruiqin Xiong, and Tiejun Huang. Optical flow estimation for spiking camera. *2022 IEEE/CVF Conference on Computer Vision and Pattern Recognition (CVPR)*, 6 2022. 3
- [18] Y Hu, S C Liu, and T Delbruck. v2e: From video frames to realistic DVS events. In *2021 IEEE/CVF Conference on Computer Vision and Pattern Recognition Workshops (CVPRW)*. IEEE, 2021. 2
- [19] Tak-Wai Hui, Xiaou Tang, and Chen Change Loy. LiteFlowNet: A Lightweight Convolutional Neural Network for Optical Flow Estimation. In *Proceedings of IEEE Conference on Computer Vision and Pattern Recognition (CVPR)*, pages 8981–8989, 2018. 2, 3
- [20] Junhwa Hur and Stefan Roth. Iterative residual refinement for joint optical flow and occlusion estimation. In *2019 IEEE/CVF Conference on Computer Vision and Pattern Recognition (CVPR)*, pages 5747–5756, 2019. 3
- [21] Eddy Ilg, Nikolaus Mayer, Tonmoy Saikia, Margret Keuper, Alexey Dosovitskiy, and Thomas Brox. FlowNet 2.0: Evolution of optical flow estimation with deep networks. *2017 IEEE Conference on Computer Vision and Pattern Recognition (CVPR)*, Jul 2017. 3
- [22] Huaizu Jiang, Deqing Sun, Varan Jampani, Ming-Hsuan Yang, Erik Learned-Miller, and Jan Kautz. Super sloMo: High quality estimation of multiple intermediate frames for video interpolation. *2018 IEEE/CVF Conference on Computer Vision and Pattern Recognition*, 1 2018. 1
- [23] Shihao Jiang, Yao Lu, Hongdong Li, and Richard I. Hartley. Learning optical flow from a few matches. *2021 IEEE/CVF Conference on Computer Vision and Pattern Recognition (CVPR)*, pages 16587–16595, 2021. 2, 3, 6
- [24] Diederik P. Kingma and Jimmy Ba. Adam: A method for stochastic optimization. In Yoshua Bengio and Yann LeCun,

- editors, *3rd International Conference on Learning Representations, ICLR 2015, San Diego, CA, USA, May 7-9, 2015, Conference Track Proceedings*, 2015. 5
- [25] Zhuoyan Li, Jiawei Shen, and Ruitao Liu. A lightweight network to learn optical flow from event data. In *2020 25th International Conference on Pattern Recognition (ICPR)*, pages 1–7, 2021. 3
- [26] Guo Lu, Xiaoyun Zhang, Wanli Ouyang, Li Chen, Zhiyong Gao, and Dong Xu. An end-to-end learning framework for video compression. *IEEE Transactions on Pattern Analysis and Machine Intelligence*, 43(10):3292–3308, 2021. 1
- [27] Yao Lu, Jack Valmadre, Heng Wang, Juho Kannala, Mehrtash Harandi, and Philip H. S. Torr. Devon: Deformable volume network for learning optical flow. *2020 IEEE Winter Conference on Applications of Computer Vision (WACV)*, Mar 2020. 3
- [28] Bruce D. Lucas and Takeo Kanade. An iterative image registration technique with an application to stereo vision. In *Proceedings of the 7th International Joint Conference on Artificial Intelligence - Volume 2, IJCAI’81*, page 674–679, San Francisco, CA, USA, 1981. Morgan Kaufmann Publishers Inc. 1, 2, 3
- [29] Elias Mueggler, Christian Forster, Nathan Baumli, Guillermo Gallego, and Davide Scaramuzza. Lifetime estimation of events from dynamic vision sensors. In *2015 IEEE International Conference on Robotics and Automation (ICRA)*, pages 4874–4881, 2015. 2
- [30] Michal Neoral, Jan Šochman, and Jiří Matas. Continual occlusion and optical flow estimation. In C.V. Jawahar, Hongdong Li, Greg Mori, and Konrad Schindler, editors, *Computer Vision – ACCV 2018*, pages 159–174, Cham, 2019. Springer International Publishing. 3
- [31] Federico Paredes-Valles and Guido C. H. E. de Croon. Back to event basics: Self-supervised learning of image reconstruction for event cameras via photometric constancy. In *Proceedings of the IEEE/CVF Conference on Computer Vision and Pattern Recognition (CVPR)*, pages 3446–3455, June 2021. 2
- [32] Adam Paszke, Sam Gross, Francisco Massa, Adam Lerer, James Bradbury, Gregory Chanan, Trevor Killeen, Zeming Lin, Natalia Gimelshein, Luca Antiga, Alban Desmaison, Andreas Köpf, Edward Yang, Zach DeVito, Martin Raison, Alykhan Tejani, Sasank Chilamkurthy, Benoit Steiner, Lu Fang, Junjie Bai, and Soumith Chintala. Pytorch: An imperative style, high-performance deep learning library, 2019. 5
- [33] Tong Qin, Peiliang Li, and Shaojie Shen. Vins-mono: A robust and versatile monocular visual-inertial state estimator. *IEEE Transactions on Robotics*, 34(4):1004–1020, 2018. 1
- [34] Anurag Ranjan and Michael J. Black. Optical flow estimation using a spatial pyramid network. In *Proceedings of the IEEE Conference on Computer Vision and Pattern Recognition*, 2017. 2, 3
- [35] Rajesh P. N. Rao and Dana H. Ballard. Predictive coding in the visual cortex: a functional interpretation of some extra-classical receptive-field effects. *Nature Neuroscience*, 2(1):79–87, 1999. 4
- [36] Shintaro Shiba, Yoshimitsu Aoki, and Guillermo Gallego. Secrets of event-based optical flow. In *European Conference on Computer Vision (ECCV)*, 2022. 2, 6
- [37] Leslie N. Smith and Nicholay Topin. Super-convergence: very fast training of neural networks using large learning rates. *Artificial Intelligence and Machine Learning for Multi-Domain Operations Applications*, May 2019. 5
- [38] Deqing Sun, Xiaodong Yang, Ming-Yu Liu, and Jan Kautz. Pwc-net: Cnns for optical flow using pyramid, warping, and cost volume. *2018 IEEE/CVF Conference on Computer Vision and Pattern Recognition*, Jun 2018. 1, 2, 3
- [39] GreenWaves Technologies. Memory issues for ai edge chips. [https://greenwaves-technologies.com/gap9\\_processor/](https://greenwaves-technologies.com/gap9_processor/), Jan 2023. 13
- [40] Gyr Falcon Technology. Memory issues for ai edge chips. <https://www.gyrfalcontech.ai/solutions/lightspeur-5801/>, May 2020. 13
- [41] Zachary Teed and Jia Deng. Raft: Recurrent all-pairs field transforms for optical flow. In Andrea Vedaldi, Horst Bischof, Thomas Brox, and Jan-Michael Frahm, editors, *Computer Vision – ECCV 2020*, pages 402–419, Cham, 2020. Springer International Publishing. 1, 2, 3, 5
- [42] Longguang Wang, Yulan Guo, Li Liu, Zaiping Lin, Xinpu Deng, and Wei An. Deep video super-resolution using hr optical flow estimation. *IEEE Transactions on Image Processing*, 29:4323–4336, 2020. 1
- [43] Jian Xiong, Hongliang Li, Qingbo Wu, and Fanman Meng. A fast hevcc inter cu selection method based on pyramid motion divergence. *IEEE Transactions on Multimedia*, 16(2):559–564, 2014. 1
- [44] Hao-fei Xu, Jiaolong Yang, Jianfei Cai, Juyong Zhang, and Xin Tong. High-resolution optical flow from 1d attention and correlation. In *Proceedings of the IEEE/CVF International Conference on Computer Vision*, pages 10498–10507, 2021. 2, 3, 6
- [45] Chengxi Ye, Anton Mitrokhin, Cornelia Fermüller, James A. Yorke, and Yiannis Aloimonos. Unsupervised learning of dense optical flow, depth and egomotion with event-based sensors. In *2020 IEEE/RSJ International Conference on Intelligent Robots and Systems (IROS)*, pages 5831–5838, 2020. 2, 3
- [46] Alex Zhu, Liangzhe Yuan, Kenneth Chaney, and Kostas Daniilidis. Ev-flownet: Self-supervised optical flow estimation for event-based cameras. *Robotics: Science and Systems XIV*, Jun 2018. 2, 6, 7
- [47] Alex Zihao Zhu, Dinesh Thakur, Tolga Özaslan, Bernd Pfrommer, Vijay Kumar, and Kostas Daniilidis. The multivehicle stereo event camera dataset: An event camera dataset for 3d perception. *IEEE Robotics and Automation Letters*, 3(3):2032–2039, 2018. 2
- [48] Alex Zihao Zhu, Liangzhe Yuan, Kenneth Chaney, and Kostas Daniilidis. Unsupervised event-based learning of optical flow, depth, and egomotion. *2019 IEEE/CVF Conference on Computer Vision and Pattern Recognition (CVPR)*, 6 2019. 3



## A. Optical Flow Coding Scheme

The visualizations of optical flow used in the figures are created by mapping the magnitude and direction of optical flow vectors into brightness and colour hue respectively as shown in Fig. 6. The brightness in the colours is normalized according to the maximum optical flow magnitude given by E-RAFT predictions and the same scale is applied to all predictions made by other models. The difference map uses a scale normalized to a maximum optical flow magnitude of 30 pixels to magnify the discrepancies between different predictions.

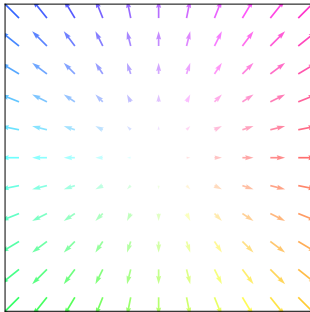


Figure 6. Optical flow coding scheme. The magnitude and direction of optical flow vectors are encoded in brightness and colour hue respectively.

## B. Event Coding Scheme

The visualizations of events used in the figures are created by mapping positive and negative polarity events into colour hues and intensity as shown in Fig. 7.



Figure 7. Event coding scheme. Negative events are mapped to cyan and positive events are mapped to purple. Pixels with both positive and negative events exhibit a mix of the two colours, resulting in different shades of blue.

## C. Ablation Studies on the Impact of Feature Map Resolutions

Presented in Table 6, we experimentally examine how feature map resolutions affect model performance. We conducted a study where we increased the feature map resolution from 1/8th to 1/4th of the input event resolution while keeping all other elements unchanged.

	Feature Map Resolution	EPE	AE	Memory Footprint
E-RAFT [13]	1/8	<u>0.79</u>	2.85	132MB
	1/4	-	-	1.9GB
Non-recurrent E-RAFT [13]	1/8	<u>0.84</u>	2.95	132MB
	1/4	<u>0.79</u>	<u>2.83</u>	1.9GB
<b>Ours, ID</b>	1/8	<u>0.79</u>	2.91	<b>20MB</b>
	1/4	<b>0.72</b>	<b>2.72</b>	<u>30MB</u>

Table 6. Ablation studies on DSEC-Flow w.r.t the impact of performance by feature map resolution. Training the recurrent version of E-RAFT with upscaled feature maps was infeasible due to excessive memory usage.

Although the recurrent E-RAFT (with warm starting) cannot fit in a single GPU for training with an upscaled feature map, we were able to train the non-recurrent E-RAFT despite it barely fitting in the GPU memory with cropped inputs. The results indicate that using 1/4th resolution feature maps to construct the correlation volume, as opposed to the original model’s 1/8th resolution, led to a 6% reduction in EPE. This is consistent with our findings on *IDNet* where a slightly larger 9% reduction is similarly observed. However, we would like to highlight that our approach has superior memory usage compared to correlation volumes and scales very well to higher-resolution input while any attempts to further increase the resolution (input or augmented crops) will lead to prohibitively high memory costs for correlation-based methods.

## D. Network Architecture

*IDNet* under *ID* and *TID* schemes share the same RNN backbone and `Encoder` architecture. Each slice of event bin  $\mathcal{E}$  of size  $1 \times H \times W$  is first encoded into 64-dim feature maps of 1/8th or 1/4th lower-resolution through the layers of the `Encoder` module shown in Table 7 and Table 8.

Next, the encoded feature maps are processed by the backbone RNN which consists of a single `ConvGRU` layer, as shown in Table 9. The internal state of `ConvGRU` layer has 96 channels for *ID* and *TID* at 1/8 resolution. In the case of *ID* with 1/4 resolution, the number of channels is increased to 128. Lastly, the flow prediction is read out from the state (memory) of the RNN through the readout module shown in Table 10. The final optical flow is upsampled from a lower-resolution flow map using an upsampling mask retrieved from the RNN memory.

For *TID*, an additional future flow is estimated through a separately instantiated readout module which shares the same architecture. `WSM` module shares the same architecture as the `Encoder` module shown in Table 7 except for the input shape of the first layer being  $2 \times H \times W$ .

Note the GMACs in Table 7, Table 9 and Table 10 are based on a single event bin of 640 by 480 pixels.

Layer	Input Shape	Output Shape	# Parameters	GMAC
Conv2D (Kernel size = 7, Stride = 2) w/ ReLU	1, H, W	32, H/2, W/2	3,168	0.243
1/8 Resolution:				
Residual Block 1 ( $C_{out} = 32$ , Stride = 2)	32, H/2, W/2	32, H/4, W/4	19,552	0.375
Residual Block 2 ( $C_{out} = 32$ , Stride = 1)	32, H/4, W/4	32, H/4, W/4	18,496	0.355
Residual Block 3 ( $C_{out} = 64$ , Stride = 2)	32, H/4, W/4	64, H/8, W/8	57,536	0.276
Residual Block 4 ( $C_{out} = 64$ , Stride = 1)	64, H/8, W/8	64, H/8, W/8	73,856	0.354
1/4 Resolution:				
Residual Block 1 ( $C_{out} = 64$ , Stride = 2)	32, H/2, W/2	64, H/4, W/4	57,536	1.104
Residual Block 2 ( $C_{out} = 64$ , Stride = 1)	64, H/4, W/4	64, H/4, W/4	73,856	1.418
Residual Block 3 ( $C_{out} = 64$ , Stride = 1)	64, H/4, W/4	64, H/4, W/4	73,856	1.418
Residual Block 4 ( $C_{out} = 64$ , Stride = 1)	64, H/4, W/4	64, H/4, W/4	73,856	1.418

Table 7. Layer details of the Encoder module.

Layer	Input Shape	Output Shape
Conv2D (Kernel size = 3, Stride = S) w/ ReLU	$C_{in}$ , H, W	$C_{out}$ , H/S, W/S
Conv2D (Kernel size = 3, Stride = 1) w/ ReLU	$C_{out}$ , H/S, W/S	$C_{out}$ , H/S, W/S

Table 8. Layer details of a residual block with stride S and output channel  $C_{out}$ .

Layer	Input Shape	Output Shape	# Parameters	GMAC
1/8 Resolution:				
ConvGRU	96+64, H/8, W/8	96, H/8, W/8	415,008	1.992
1/4 Resolution:				
ConvGRU	128+64, H/4, W/4	128, H/4, W/4	221,312	12.74

Table 9. Layer details of the RNN backbone.

Layer	Input Shape	Output Shape	# Parameters	GMAC
Low-resolution flow:				
Conv2D (Kernel size = 3)	64, H/8, W/8	64, H/4, W/4	36,928	0.177
ReLU	64, H/8, W/8	64, H/8, W/8	-	-
Conv2D (Kernel size = 3)	64, H/8, W/8	2, H/8, W/8	1,154	0.005
Upsample mask:				
Conv2D (Kernel size = 3)	64, H/8, W/8	256, H/4, W/4	147,712	0.709
ReLU	256, H/8, W/8	256, H/8, W/8	-	-
Conv2D (Kernel size = 3)	256, H/8, W/8	576, H/8, W/8	148,032	0.710
Upsampled Flow:				
Conv Upsampling	2, H/8, W/8 576, H/8, W/8	2, H, W	-	0.002

Table 10. Layer details of the memory readout module for 1/8 resolution. The same layers apply while their input and mask dimensions are adjusted accordingly to handle the case of 1/4 resolution.

## E. Motivation for Low-memory, Low-latency Models

Complemented by the low power of event cameras compared to frame-based ones (10 mW vs. 1W), we envision the biggest use cases for power-constrained embedded systems such as IoT and robotic platforms, especially those whose power budget is only a few hundred milliwatts. This precludes the use of mobile GPUs such as Jetson Nano using over 5W. As a concrete example, we provide in Table 11 specs of two recently launched edge compute devices: 1) GAP 9 processor which is used to accelerate inference on-board tiny Crazyflie drones (7W for flight), and 2) Gyr Falcon 5801 accelerator optimized for CNN inference as well as their expected FPS when running our methods.

	GAP 9[39]	Gyr Falcon 5801[40]
Processing Power	0.15 TOPs	2.8 TOPs
Power Efficiency	330 mW/TOPs	80 mW/TOPs
Max Memory	16 MB	10 MB
Peak Power	50 mW	224 mW
E-RAFT FPS	Insufficient Memory	
ID/TID FPS	0.7 / 2.7	12 / 50

Table 11. Performance of typical embedded AI inference chip.

While E-RAFT well exceeds the memory capacity of these accelerators, *IDNet* fits on these platforms using 16-bit float representation. These accelerators typically combine low-density and expensive memory such as SRAM and in/near-memory computing to maximize power efficiency. Hence, their memory becomes a scarce and cost-sensitive resource and is generally limited to a few tens of MB [8]. The other use cases are for low-latency applications, such as robots that need to act fast in dynamic environments, e.g., event-based high-speed landings [15]. Even on more powerful systems, fast algorithms are always good as it enables more simultaneous tasks. A robot will only become useful when performing more than optical flow alone.

## F. Detailed Quantitative Results

Per-sequence breakdown of the quantitative results is available in Table 12.

## G. Additional Qualitative Results

Additional qualitative results on DSEC-Flow [12] is provided in Fig. 8, Fig. 9, Fig. 10, Fig. 11 and Fig. 12. Regions of interest which show differences in predictions are highlighted in red square. Note, the difference map is created against E-RAFT. However, large differences should not be interpreted as prediction error by default, as our *ID* (1/4 Res) model produces more accurate optical flow estimates than E-RAFT for most cases. Our *TID*

model slightly underperforms E-RAFT in terms of producing blurry motion boundaries. Additionally, it occasionally fails to predict flow accurately when objects move out of the scene, as seen by trails in `zurich_city_14_c` (569). However, it should be noted that this is not always the case, as demonstrated in `interlaken_01_a` (892) and `interlaken_00_b` (745).

interlaken_00_b					
	EPE	AE	1PE	2PE	3PE
E-RAFT [13]	<u>1.39</u>	2.36	20.4	9.4	6.2
<b>Ours (ID, 1/4 Res)</b>	<b>1.25</b>	<b>2.11</b>	<b>14.1</b>	<b>6.5</b>	<b>4.4</b>
<b>Ours (ID, 1/8 Res)</b>	1.43	<u>2.31</u>	<u>17.5</u>	<u>8.3</u>	<u>5.6</u>
<b>Ours (TID)</b>	1.43	2.85	25.7	10.5	6.3
ID (1 iteration)	2.30	3.87	43.1	23.5	15.6
ID (2 iterations)	1.67	2.95	25.1	12.4	8.4
ID (4 iters w/o deblurring)	2.19	4.09	45.0	25.2	15.7
ID (4 iters w/o WSM)	1.96	3.31	31.3	15.6	10.7

thun_01_a					
	EPE	AE	1PE	2PE	3PE
E-RAFT [13]	0.65	2.94	11.0	3.5	1.9
<b>Ours (ID, 1/4 Res)</b>	<b>0.57</b>	<b>2.66</b>	<b>6.7</b>	<b>2.6</b>	<b>1.5</b>
<b>Ours (ID, 1/8 Res)</b>	<u>0.61</u>	<u>2.70</u>	<u>9.0</u>	<u>3.2</u>	<u>1.8</u>
<b>Ours (TID)</b>	0.73	3.31	12.8	4.3	2.6
ID (1 iteration)	1.04	4.71	28.6	9.2	4.5
ID (2 iterations)	0.77	3.28	15.0	5.4	2.9
ID (4 iters w/o deblurring)	0.97	4.08	24.5	8.2	4.0
ID (4 iters w/o WSM)	0.75	3.34	15.3	4.9	2.4

zurich_city_12_a					
	EPE	AE	1PE	2PE	3PE
E-RAFT [13]	<u>0.61</u>	<b>4.50</b>	<u>11.2</u>	<u>2.4</u>	<b>1.1</b>
<b>Ours (ID, 1/4 Res)</b>	<b>0.60</b>	<u>4.56</u>	<b>10.8</b>	<b>2.3</b>	<b>1.1</b>
<b>Ours (ID, 1/8 Res)</b>	0.63	4.78	12.0	2.7	1.4
<b>Ours (TID)</b>	0.67	5.37	13.7	2.7	<u>1.3</u>
ID (1 iteration)	1.01	8.08	34.0	7.3	2.9
ID (2 iterations)	0.74	5.31	17.2	4.0	1.8
ID (4 iters w/o deblurring)	0.93	6.87	28.7	6.4	2.4
ID (4 iters w/o WSM)	0.81	6.56	22.1	4.4	1.8

zurich_city_15_a					
	EPE	AE	1PE	2PE	3PE
E-RAFT [13]	<u>0.59</u>	<b>2.55</b>	8.8	2.6	1.3
<b>Ours (ID, 1/4 Res)</b>	<b>0.55</b>	<b>2.55</b>	<b>6.8</b>	<b>1.9</b>	<b>1.0</b>
<b>Ours (ID, 1/8 Res)</b>	<u>0.59</u>	<u>2.65</u>	<u>8.5</u>	<u>2.4</u>	<u>1.2</u>
<b>Ours (TID)</b>	0.65	3.06	10.0	2.7	1.3
ID (1 iteration)	1.00	4.32	27.8	8.3	3.7
ID (2 iterations)	0.73	3.17	14.1	4.3	2.1
ID (4 iters w/o deblurring)	0.92	3.99	23.3	7.1	3.1
ID (4 iters w/o WSM)	0.75	3.69	15.5	3.7	<u>1.7</u>

interlaken_01_a					
	EPE	AE	1PE	2PE	3PE
E-RAFT [13]	0.90	2.54	15.5	6.8	3.9
<b>Ours (ID, 1/4 Res)</b>	<b>0.77</b>	<b>2.25</b>	<b>11.6</b>	<b>4.5</b>	<b>2.6</b>
<b>Ours (ID, 1/8 Res)</b>	<u>0.85</u>	<u>2.47</u>	<u>14.2</u>	<u>5.6</u>	<u>3.2</u>
<b>Ours (TID)</b>	0.93	2.88	16.7	6.3	3.5
ID (1 iteration)	1.44	4.08	38.6	17.1	9.2
ID (2 iterations)	1.01	2.97	20.6	8.4	4.6
ID (4 iters w/o deblurring)	1.45	4.11	38.2	17.3	9.8
ID (4 iters w/o WSM)	3.71	1.07	22.8	9.1	5.1

thun_01_b					
	EPE	AE	1PE	2PE	3PE
E-RAFT [13]	<u>0.58</u>	<u>2.20</u>	<u>8.3</u>	<u>2.9</u>	<u>1.5</u>
<b>Ours (ID, 1/4 Res)</b>	<b>0.55</b>	<b>2.07</b>	<b>6.7</b>	<b>2.4</b>	<b>1.4</b>
<b>Ours (ID, 1/8 Res)</b>	0.61	2.28	8.8	3.0	1.6
<b>Ours (TID)</b>	0.65	2.59	10.3	3.2	1.7
ID (1 iteration)	0.97	3.81	25.9	8.8	3.9
ID (2 iterations)	0.73	2.69	14.0	4.7	2.4
ID (4 iters w/o deblurring)	0.90	3.54	21.3	7.1	3.1
ID (4 iters w/o WSM)	0.75	3.13	14.6	4.5	2.2

zurich_city_14_c					
	EPE	AE	1PE	2PE	3PE
E-RAFT [13]	<b>0.71</b>	<b>3.43</b>	<b>15.5</b>	<b>5.1</b>	<b>1.9</b>
<b>Ours (ID, 1/4 Res)</b>	0.76	<u>3.74</u>	19.3	<u>5.9</u>	2.7
<b>Ours (ID, 1/8 Res)</b>	<u>0.74</u>	<u>3.96</u>	<u>17.3</u>	<u>6.4</u>	<u>2.1</u>
<b>Ours (TID)</b>	0.80	5.26	16.1	6.6	4.6
ID (1 iteration)	1.27	5.38	36.7	15.8	7.1
ID (2 iterations)	0.98	4.48	23.7	10.8	5.0
ID (4 iters w/o deblurring)	1.12	4.42	32.0	11.5	6.0
ID (4 iters w/o WSM)	0.92	4.62	25.8	8.2	3.4

Average					
	EPE	AE	1PE	2PE	3PE
E-RAFT [13]	<u>0.79</u>	<u>2.85</u>	12.7	4.7	2.7
<b>Ours (ID, 1/4 Res)</b>	<b>0.72</b>	<b>2.72</b>	<b>10.1</b>	<b>3.5</b>	<b>2.0</b>
<b>Ours (ID, 1/8 Res)</b>	<u>0.79</u>	2.91	<u>12.1</u>	<u>4.3</u>	<u>2.4</u>
<b>Ours (TID)</b>	0.84	3.41	14.7	5.0	2.8
ID (1 iteration)	1.30	4.82	33.7	12.8	6.7
ID (2 iterations)	0.94	3.43	18.1	6.7	3.7
ID (4 iters w/o deblurring)	1.24	4.49	31.1	12.3	6.6
ID (4 iters w/o WSM)	1.02	4.07	20.8	7.2	4.0

Table 12. Per sequence evaluation on DSEC-Flow dataset. The best metric is in bold, while the second best is underlined.



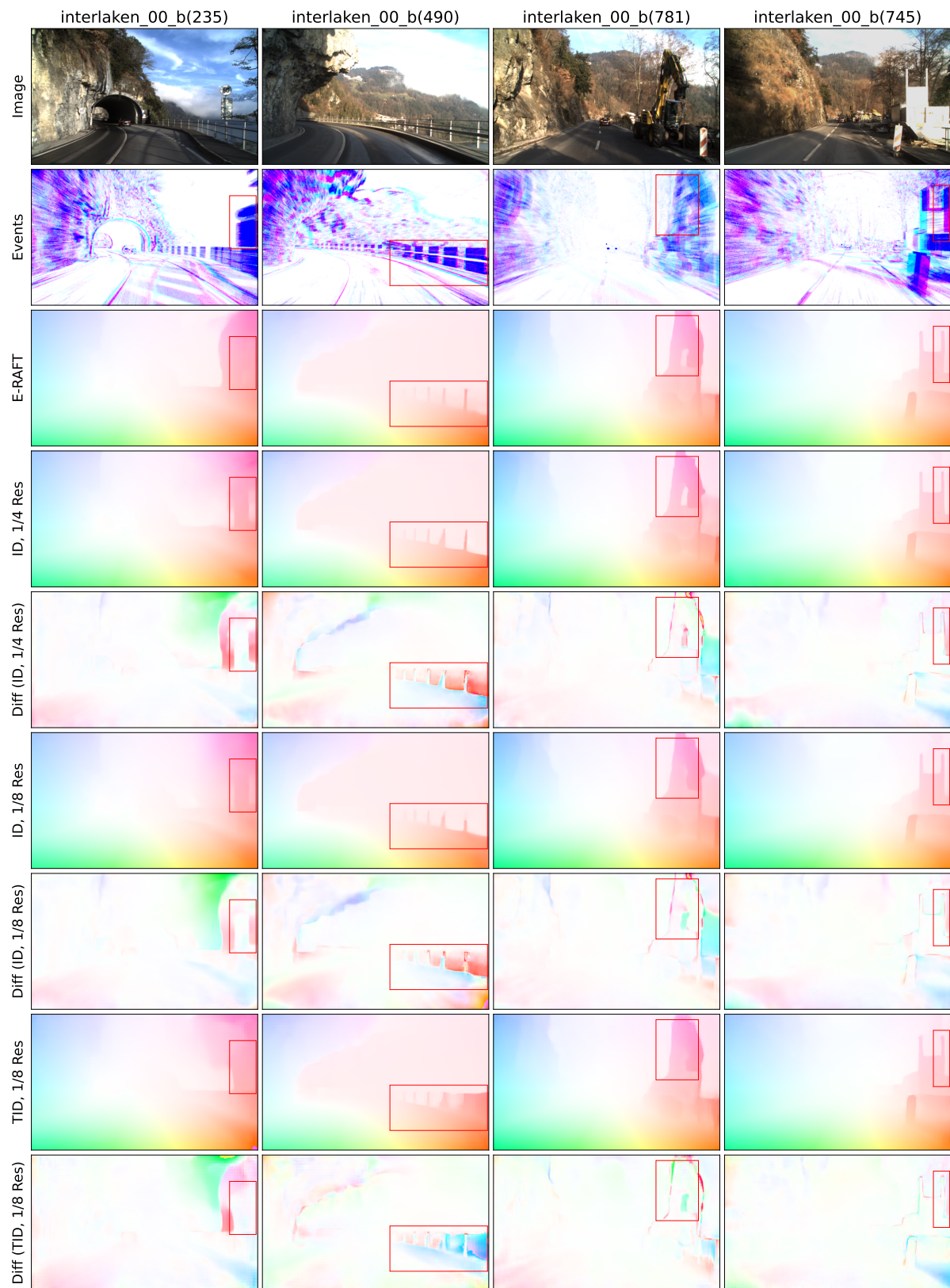


Figure 8. Additional qualitative results of samples from interlaken\_00\_b sequence.

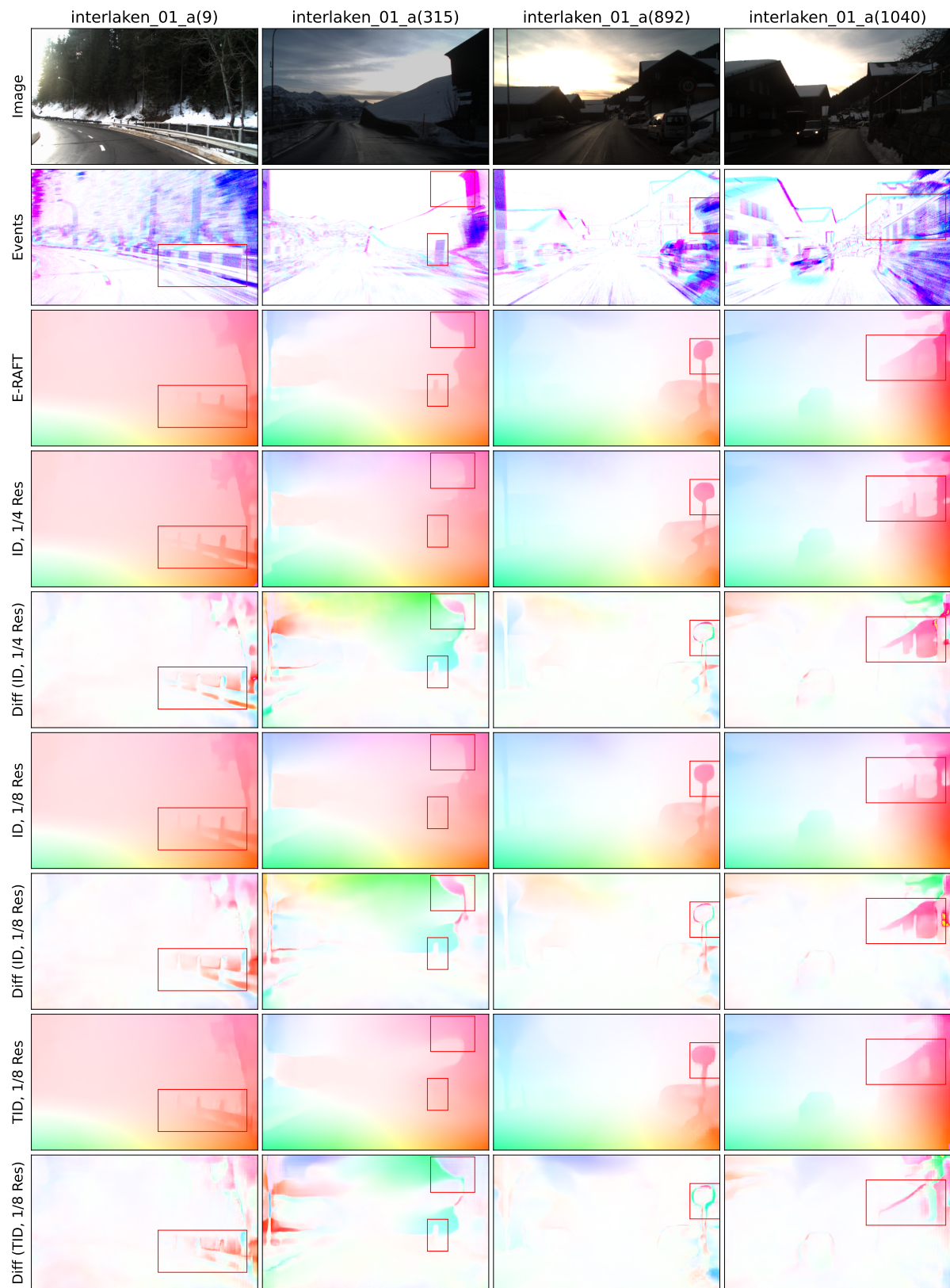


Figure 9. Additional qualitative results of samples from interlaken\_01\_a sequence.



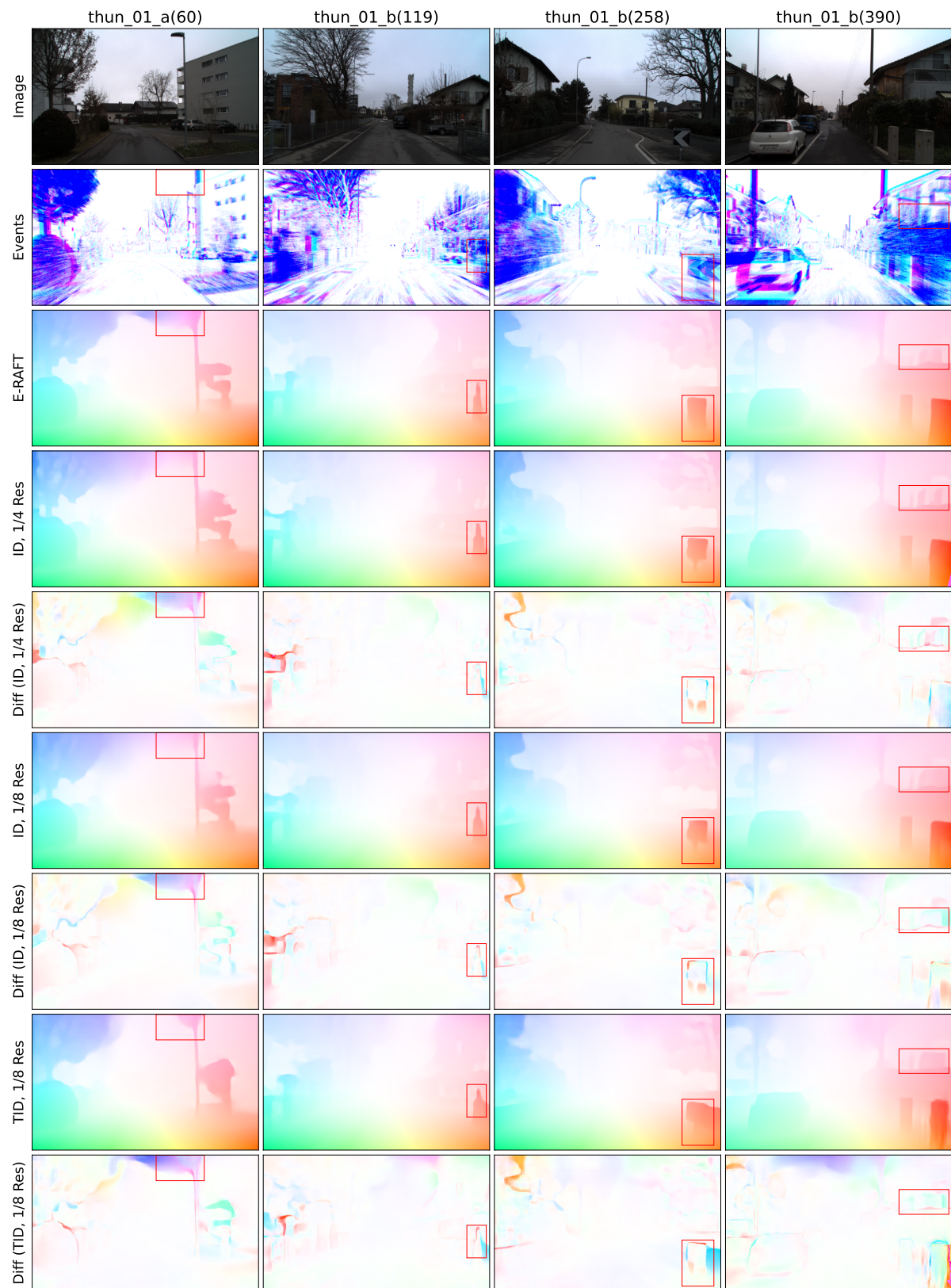


Figure 10. Additional qualitative results of samples from thun\_01.a and thun\_01.b sequence.

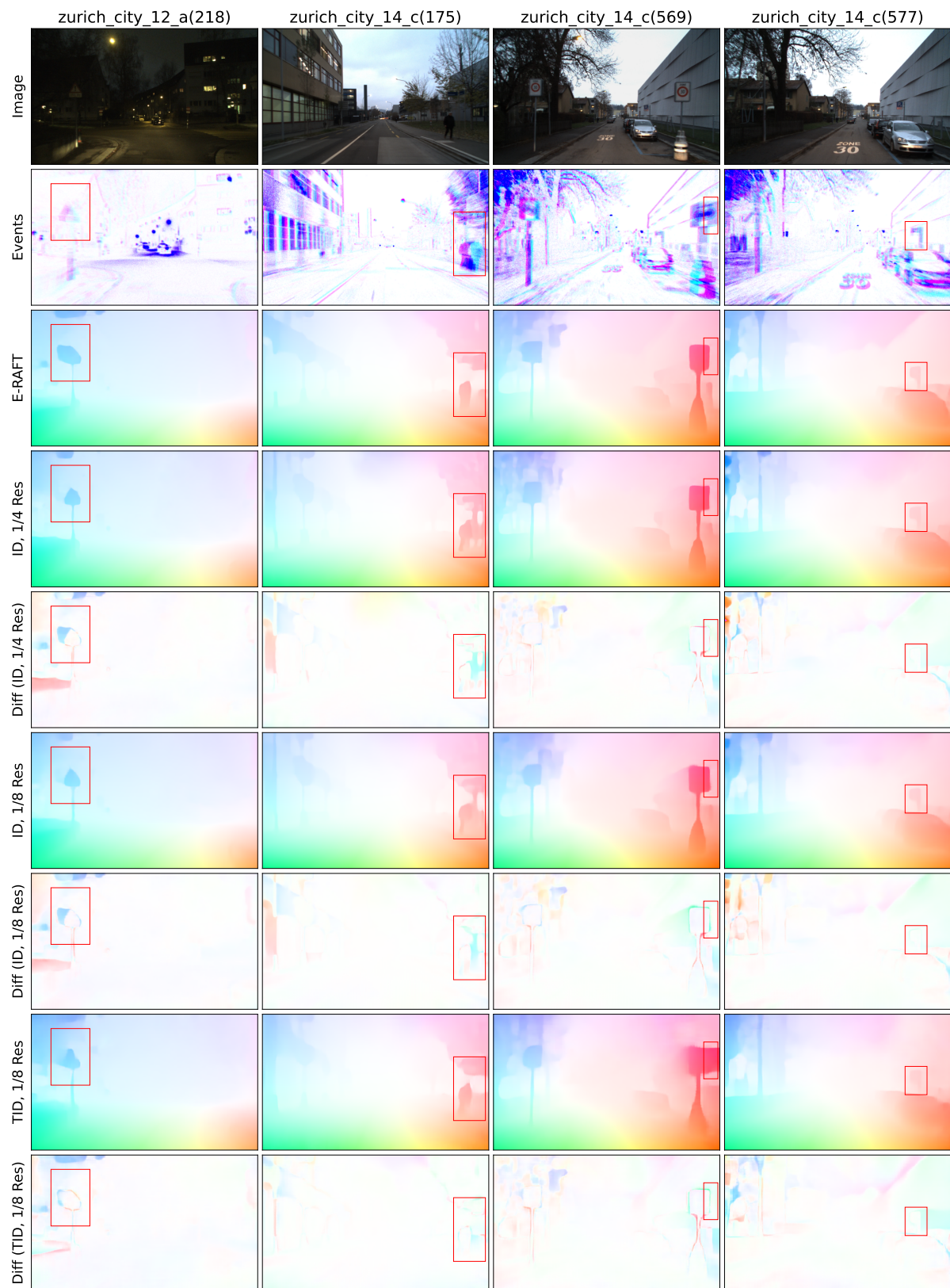


Figure 11. Additional qualitative results of samples from zurich\_city\_12.a and zurich\_city\_14.c sequence.



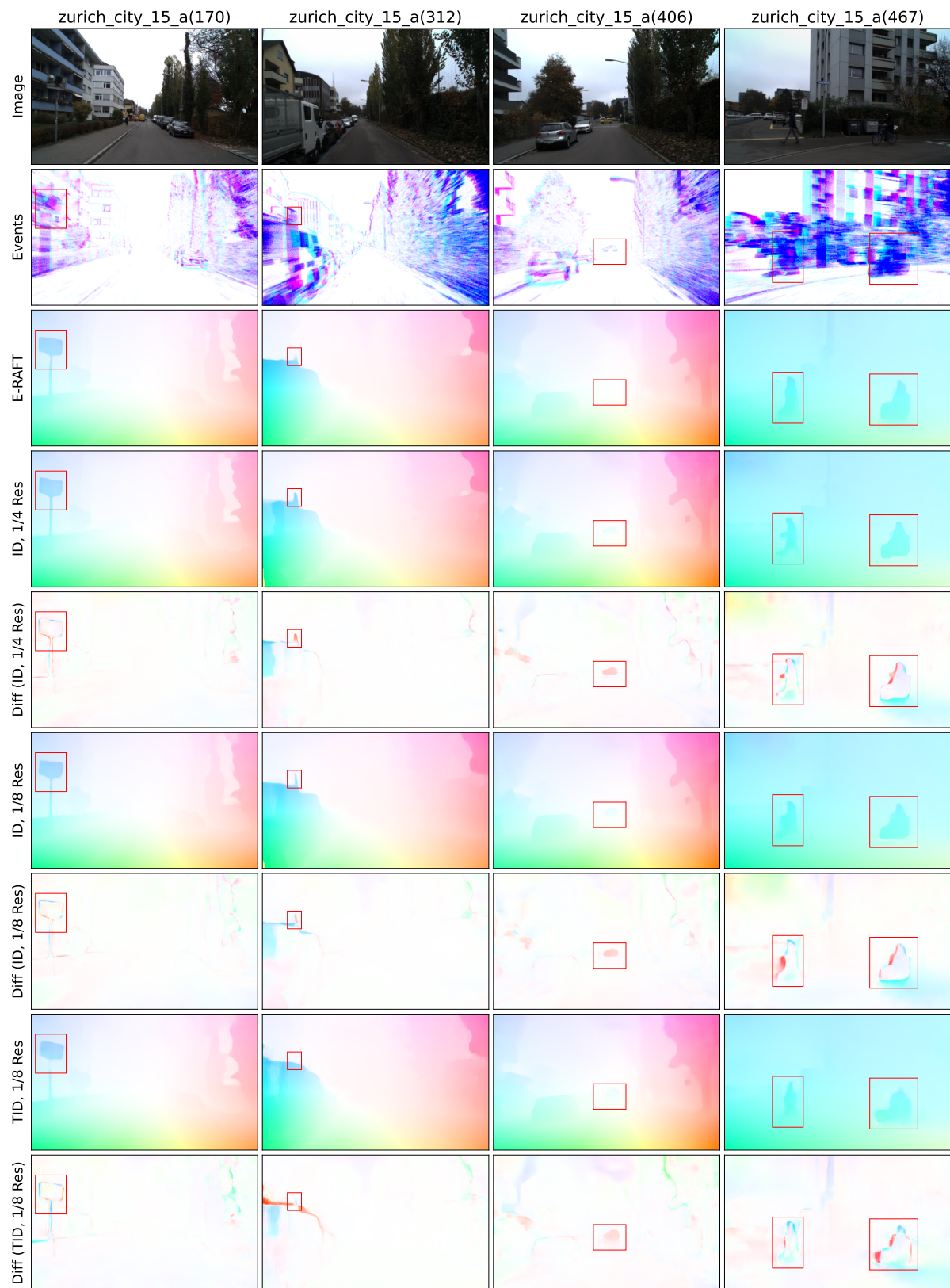


Figure 12. Additional qualitative results of samples from zurich\_city\_15\_a sequence.